



HAL
open science

Large circular dichroism in the emission by an incandescent metasurface

Anne Nguyen, Jean-Paul Hugonin, Anne-Lise Coutrot, Enrique
Garcia-Caurel, Benjamin Vest, Jean-Jacques Greffet

► **To cite this version:**

Anne Nguyen, Jean-Paul Hugonin, Anne-Lise Coutrot, Enrique Garcia-Caurel, Benjamin Vest, et al.. Large circular dichroism in the emission by an incandescent metasurface. *Optica*, 2023, 10 (2), pp.232-238. 10.1364/OPTICA.480292 . hal-03950184

HAL Id: hal-03950184

<https://hal.science/hal-03950184>

Submitted on 21 Jan 2023

HAL is a multi-disciplinary open access archive for the deposit and dissemination of scientific research documents, whether they are published or not. The documents may come from teaching and research institutions in France or abroad, or from public or private research centers.

L'archive ouverte pluridisciplinaire **HAL**, est destinée au dépôt et à la diffusion de documents scientifiques de niveau recherche, publiés ou non, émanant des établissements d'enseignement et de recherche français ou étrangers, des laboratoires publics ou privés.

To be published in Optica:

Title: Large circular dichroism in the emission by an incandescent metasurface

Authors: Anne Nguyen, Jean-Paul Hugonin, Anne-Lise Coutrot, Enrique Garcia-Caurel, benjamin vest, Jean-Jacques Greffet

Accepted: 03 January 23

Posted 04 January 23

DOI: <https://doi.org/10.1364/OPTICA.480292>

© 2023 Optica Publishing Group under the terms of the [Optica Open Access Publishing Agreement](#)

OPTICA
PUBLISHING GROUP
Formerly OSA

Large circular dichroism in the emission by an incandescent metasurface

ANNE NGUYEN,¹ JEAN-PAUL HUGONIN,¹ ANNE-LISE COUTROT,¹
ENRIQUE GARCIA-CAUREL,² BENJAMIN VEST,¹ AND JEAN-JACQUES
GREFFET,^{1,*}

¹ *Université Paris-Saclay, Institut d'Optique Graduate School, CNRS, Laboratoire Charles Fabry, 91127, Palaiseau, France*

² *LPICM, CNRS, Ecole polytechnique, Institut Polytechnique de Paris, Palaiseau, France*

**jean-jacques.greffet@institutoptique.fr*

Abstract: Compact sources in the mid-wave infrared (MWIR) are needed for several applications ranging from spectroscopy to free-space communication. Ultra-thin incandescent metasurfaces are promising candidates, offering the possibility of tuning the emission spectrum, directivity and modulation speed. However, control over polarization remains a challenge, especially when it comes to emission of circularly polarized light. Here, emission of polarized MWIR radiation by a 700 nm thick incandescent chiral metasurface is reported. The degree of polarization is above 0.5 with degree of circular polarization of 0.38 at 5 μm . The metasurface is heated by Joule effect and its emission can be modulated beyond 10 MHz. This paves the way to detection techniques using polarization as an additional degree of freedom.

© 2022 Optica Publishing Group

1. Introduction

Circularly polarized light (CPL) is uncommon in a natural environment. It was only recently discovered that few animal species are sensitive to visible CPL [1, 2] and use it to send messages to other individuals of the same species. Such signals cannot be detected by predators which are usually insensitive to polarization, similarly to commercial IR detectors. Covert communication channels in the MWIR relying on circularly polarized (CP) signals can therefore be a direct application for security or military purposes. CPL in the IR is also useful for techniques such as vibrational circular dichroism spectroscopy [3] to determine the absolute configuration of small molecules. For all these applications, sources of CPL are needed. The generation of CPL is commonly done by using a source of unpolarized light followed by a linear polarizer and a quarter wave plate optimized for the desired wavelength. However such circular polarizers can hardly be integrated in a compact system. Linear polarizers in the MWIR can be made out of thin metallic wires, namely wire grid polarizers. They can also be directly integrated with a MWIR source offering the advantage of built-in polarization selective emission, hence improved energetic efficiency. For example, it has been demonstrated that incandescent subwavelength gratings of metallic wires can emit nearly 100% linearly polarized light [4]. In contrast, the retardation element generally relies on birefringent materials, liquid crystals or total internal reflection such as in Fresnel rhombs and is therefore bulky. To obtain a retardance ϕ with a birefringent waveplate at wavelength λ between the slow and fast axes, a precise thickness $d = \lambda\phi/(2\pi\Delta n)$, Δn being the difference between the ordinary and extraordinary refractive indices, is needed. This bulkiness cannot be avoided unless a different paradigm is used. This is the goal of flat optics or metasurfaces, a field that has recently gained considerable interest for the miniaturization of optical elements. Many devices with differentiated CP responses based on subwavelength unit cells with structural chirality have been explored. Recent reviews [5–7] provide an overview of the state-of-the-art in terms of metamaterials and metasurfaces for polarization control.

Initial interest grew in CP selective filters. Using concepts developed in the framework of

46 nanophotonics, 3D chiral photonic crystals have been considered as efficient CP sensitive filters
47 as they can have a photonic polarization-dependent stop-band. Noticeable circular dichroism
48 (CD) was theoretically predicted in arrays of helices standing in a dielectric background [8].
49 Experimental evidence was shown in transmission for dielectric [9] helices in the NIR or
50 for metallic helices in the mid infrared [10], achieving up to 0.95 CD, and in reflection
51 in the visible [11] with 0.64 peak CD. As fabrication procedures to build such continuous
52 twisted structures are complex, a discretized alternative consisting of layers of dielectric
53 woodpiles regularly twisted with respect to each other was proposed [12] and demonstrated
54 experimentally [13] in the NIR. Stacks of arrays of twisted split ring resonators [14] has been
55 demonstrated in the MWIR. Experiments in the visible [15] with twisted photonic crystals using a
56 number of layers on the order of 10 have also been reported. However, for enhanced compactness
57 and minimal fabrication steps, chiral planar metasurfaces are highly desirable.

58 Such metasurfaces were first reported in [16] where linear-to-circular polarization conversion
59 in reflection occurs on 2D metallic array of gammadions with an opposite ellipticity of light
60 depending on the orientation of the gammadions. Polarization converters were also proposed [17],
61 using a meanderline metallic metasurface as a broadband polarization converter in reflection in
62 the LWIR to obtain CP light from a linearly polarized impinging beam. Dielectric metasurfaces
63 have also been used for polarization conversion in transmission [18].

64 Interest also emerged for chiral metasurfaces to build CP-sensitive detectors. [19] proposed
65 an Archimedean spiral composed of thermocouples as a CP sensitive detector in the LWIR.
66 Local absorption occurs at different locations, resulting in temperature differences that induce
67 a different voltage. Plasmonic zigzag-shaped metamaterials can also behave as CP selective
68 absorbers [20–22]. [20] and [22] obtain similar levels of dichroism with a 0.7 peak contrast in
69 absorption in the NIR.

70 As for CP emission, seldom solutions have been proposed up to now. It has been suggested [23]
71 that spontaneous emission could not produce circularly polarized light due to the fact that random
72 thermal current densities along two axis are uncorrelated according to fluctuation-dissipation
73 theorem for an isotropic medium. As a consequence, they could not generate polarized fields.
74 While this is the case for emission in a homogeneous and isotropic medium, when emission is
75 mediated by a resonator or cavity the emission process is different. Fluctuating current densities
76 excite the resonator or cavity modes generating induced current densities which then radiate.
77 These induced current densities can radiate circularly polarized fields. A well-known example
78 illustrating the difference between fluctuating currents and induced currents is thermal emission by
79 a grating supporting surface phonon polaritons [24]. The induced currents generate a directional
80 emission. Similarly, polarized emission may occur when designing surfaces sustaining modes
81 with appropriate correlations of the induced current densities components.

82 These ideas have been implemented a few times in the visible and NIR range. Quantum
83 dots embedded in the middle of a chiral 3D photonic crystal [25,26] show a degree of circular
84 polarization (DOCP) up to 0.5. A variant with quantum dots lying beneath arrays of planar
85 gammadions [27] show a DOCP of 0.2 at best.

86 The field of incandescent sources of circularly polarized radiation is still in its infancy.
87 A procedure to design thermal metasurfaces with a large degree of polarization has been
88 proposed [28] but not yet implemented experimentally. To the best of our knowledge, circular
89 emission was first reported using metasurfaces based on geometric phase engineering allowing
90 spin-orbit interaction [29]. This proof of principle did not report quantitative characterization. A
91 qualitative result was also reported in ref. [30] using an array of tripodes. Generation of circular
92 polarization was reported by shaping unpolarized emission by a blackbody emitter using wire
93 grid polarizers to generate linearly polarized LWIR radiation followed by a linear-to-circular
94 polarization converter [23, 30]. The device achieves a 0.28 DOCP with a total degree of
95 polarization of 0.84. Although these sources are less than 1.5 μm thick, they still need an

96 intermediate step for polarization conversion which leads to a reduced device efficiency. A recent
 97 preprint reports a thermal metasurface producing a DOCP of 0.4 [31]. In summary, while there
 98 are many reports demonstrating thermal metasurfaces controlling the emission direction, the
 99 emission spectrum, emitting linearly polarized light, the emission of pure circularly polarized
 100 thermal radiation by a metasurface is still a challenge.

101 In this paper, we introduce an incandescent metasurface optimized for the MWIR that emits
 102 circularly polarized light with a degree of polarization (DOP) larger than 0.5 on a large spectral
 103 range from 5 to 7 μm . A large circular dichroism (CD) of 0.38 is reached at 5 μm . To analyze
 104 theoretically the origin of the CD, we study the quasinormal modes of the structure and find a
 105 large difference in their coupling to each helicity of circular polarization. In contrast with sources
 106 that have been reported in the literature for CP emission, we use a compact metasurface (25 nm
 107 thick) which can be heated electrically and modulated up to 10 MHz. To our knowledge, no
 108 equivalent thin metasurface with controlled polarization state has been published up to now.

109 2. Results

110 2.1. Design of the device

111 We envision a metallic metasurface spectrally optimized to emit in the MWIR with a large
 112 degree of polarization where CD is dominant. Control over the spectral range of emission can
 113 be done by engineering the emissivity spectrum of the metasurface. To do this, we rely on
 114 Kirchhoff's law establishing the equality between emissivity and absorptivity [32]. To control the
 115 absorptivity spectrum, we use a Salisbury screen configuration, where an absorbing thin metallic
 116 film is deposited above a mirror at a well-chosen distance. Constructive interference between
 117 incoming and reflected wave result in a stationary wave in the medium. We can thus reach a
 118 100% absorption level at the desired wavelength by placing the metallic film at an antinode of
 119 this stationary wave [33]. Local Kirchhoff's law [34] guarantees that when heated, the same
 120 metallic film will achieve an emissivity peak close to 1. This configuration enables us to easily
 121 tune the emission peak wavelength.

122 Such a structure emits unpolarized light. To design a source that emits CPL in the normal
 123 direction, we design a metasurface with a preferential coupling to one helicity in the far-field.
 124 We texture the thin film and shape arrays of Z-shaped or half-gammadion resonators to form a
 125 chiral unit cell (see Fig. 1). We designed the device to obtain large CD in the MWIR at 4.7 μm .

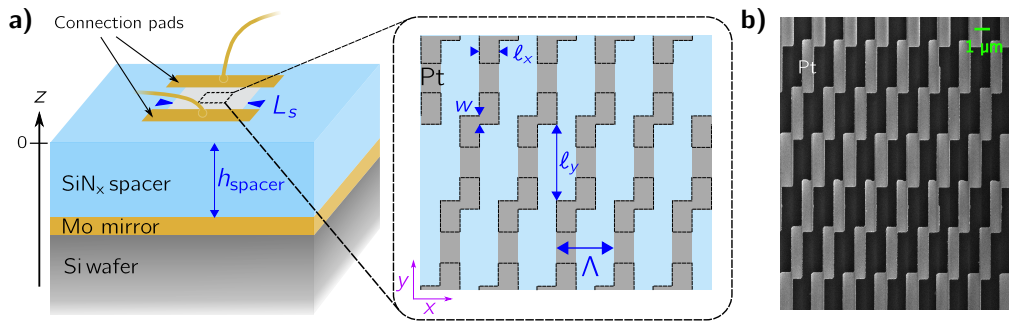


Fig. 1. a) Schematic view of the device. $l_x = 688 \text{ nm}$, $l_y = 2.737 \mu\text{m}$, $w = 300 \text{ nm}$, $\Lambda = 2.063 \mu\text{m}$, $h_{\text{spacer}} = 651 \text{ nm}$, $h_{\text{Pt}} = 25 \text{ nm}$. Dotted lines on the platinum structure serve as visual guides to mark out the Z-shaped pattern, they have no physical existence. The metasurface is $L_S \times L_S = 100 \times 100 \mu\text{m}^2$ large. b) SEM picture of the fabricated device. Scale bar, $1 \mu\text{m}$.

126 In a Salisbury configuration, the emission is due to thermally induced current density

127 fluctuations in the metallic wires. Hence, it is sufficient to heat the metasurface while leaving the
 128 substrate cold. Since the system is not isothermal, Kirchhoff's law cannot be directly used. To
 129 design the source, we make use of the local Kirchhoff's law [34] which can be used for objects
 130 with arbitrary shape and temperature field, provided that local thermodynamic equilibrium is
 131 reached. To ensure local heating, we connect the individual Z-shaped resonators to their neighbors
 132 forming nanowires as seen in Fig. 1. We deposit electrical contacts on both ends of the structure.
 133 This connected architecture can be heated locally through Joule effect by applying a voltage.
 134 Besides, as discussed in [4], this configuration enables modulation of the emitted light beyond
 135 10 MHz, five orders of magnitude faster than commercially available incandescent sources. As
 136 the structure consists of successive constrictions, the temperature increase is expected to be
 137 inhomogeneous with maxima around the constrictions. Platinum is chosen for the nanowires as
 138 it can sustain high temperatures and has a good adhesion on silicon nitride (SiN_x) [35]. We use
 139 SiN_x as the transparent spacer in the MWIR and an optically thick layer of molybdenum as the
 140 mirror, which is compatible with SiN_x . The sample was fabricated using electronic lithography
 141 as detailed in the supplemental document.

142 RCWA calculations yielding the total absorption spectrum and absorption occurring exclusively
 143 inside the platinum metasurface are shown in Fig. 2a. It is seen that absorption essentially takes
 144 place in the platinum, as expected for a Salisbury architecture.

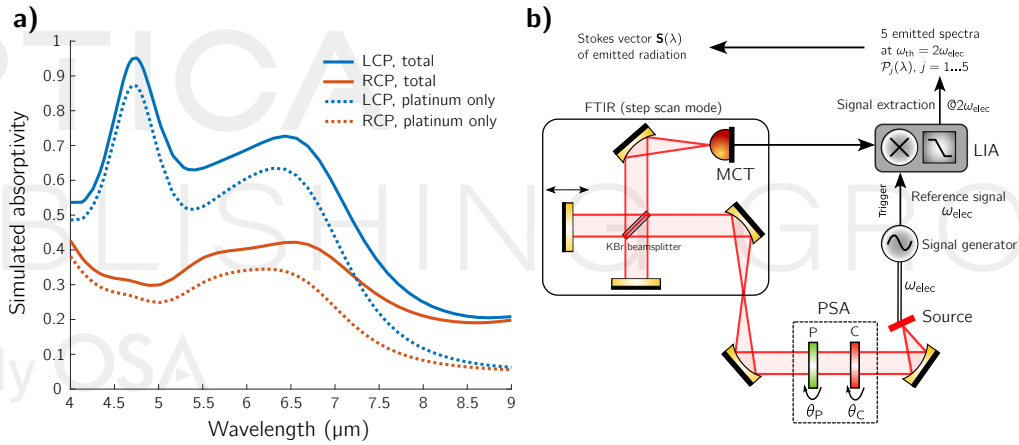


Fig. 2. a) Simulated absorption spectrum under a circularly polarized plane wave under normal incidence. Thick lines represent total absorption and dotted lines stand for absorption in the platinum structure only. b) Stokes vector characterization setup. The device is positioned in the focal plane of a collection mirror to produce a collimated beam entering the polarization state analyzer (PSA). The intensity is focused into the input slit of a FTIR. The intensity is then collected by a MCT detector. The spectrum at frequency ω_{th} is extracted with a lock-in amplifier. The operation is repeated for each of the 5 polarization projection states of the PSA.

145 2.2. Operating the source

146 In order to heat the metallic wires, we apply a sinusoidal voltage on the device with an amplitude
 147 of 13 V peak-to-peak and oscillating at frequency $\omega_{\text{elec}}/(2\pi)$. The temperature of the platinum
 148 evolves in time as $T(\mathbf{r}, t) = T_0 + T_{\text{DC}}(\mathbf{r}) + T_{\text{AC}}(\mathbf{r}, \omega_{\text{th}}) \cos(\omega_{\text{th}}t)$ with $\omega_{\text{th}} = 2\omega_{\text{elec}}$. Since
 149 the electrical resistance of platinum varies linearly with temperature, measuring the current
 150 passing through the metasurface yields its electrical resistance and hence the spatially averaged
 151 temperature. We find $T_{\text{DC}} \approx 180^\circ\text{C}$ and $T_{\text{AC}} \approx 118^\circ\text{C}$ when using $\omega_{\text{elec}}/(2\pi) = 10\text{kHz}$.
 152 Assuming that emission essentially comes from the platinum metasurface at $z = 0$, the power

153 emitted at frequency ω_{th} in a solid angle $d\Omega$ in the normal direction \mathbf{e}_z can be cast in the following
 154 form [4]:

$$P_e(\lambda, \omega_{\text{th}}, \mathbf{e}_z) \simeq d\Omega \frac{L_s^2}{2} \frac{\partial I_{\text{BB}}}{\partial T} [\lambda, T_0 + T_{\text{DC}}(z=0)] \left[A^{(\text{LCP})}(\lambda, -\mathbf{e}_z) + A^{(\text{RCP})}(\lambda, -\mathbf{e}_z) \right] \bar{T}_{\text{AC}}(\omega_{\text{th}}), \quad (1)$$

155 where I_{BB} is the blackbody radiance, $A^{(\ell)}(\lambda, \mathbf{e}_z)$ is the absorptivity under normal incidence for
 156 a circular polarization $\ell = (\text{LCP}, \text{RCP})$ and L_s is the size of the square platinum metasurface.
 157 $\bar{T}_{\text{AC}}(\omega_{\text{th}})$ is the oscillation amplitude of the temperature increase at frequency ω_{th} in the platinum,
 158 averaged over the overall platinum volume. More details on the derivation of this equation can
 159 be found in the supplemental document. The emitted light passes through a polarization state
 160 analyzer (PSA) and is measured by the spectrometer in the step scan mode. The measured output
 161 is thus proportional to $\mathcal{R}(\lambda) \mathcal{P}(\lambda) \partial I_{\text{BB}} / \partial T [\lambda, T_0 + T_{\text{DC}}(z_0)] \bar{T}_{\text{AC}}(\omega_{\text{th}})$ where $\mathcal{R}(\lambda)$ is the spectral
 162 response of the detector and $\mathcal{P}(\lambda)$ encompasses information on the polarization state selected by
 163 the PSA.

164 2.3. High frequency modulation of the incandescent source

165 In this section we show that the amplitude of the emitted power can be modulated beyond 10
 166 MHz. To characterize the source dynamic response, we modulate its temperature by applying an
 167 oscillating voltage on the electrically connected chiral platinum nanowires. The experimental
 168 setup is similar to the one described in [4]. We use a lock-in amplifier to extract the amplitude of
 169 the emitted intensity. Results are shown in Fig. 3. Two regimes can be observed as a function of
 170 the modulation frequency. In the low-frequency regime (blue shade) below 10^5 Hz, the signal
 171 amplitude is almost constant. In the high-frequency regime (pink shade), the signal decays as
 172 $1/\sqrt{\omega_{\text{th}}}$. These two regimes are dictated by the temperature dynamics of the system as discussed
 173 in [4, 36]. The signal falloff above 10 MHz is due to the detector frequency cutoff.

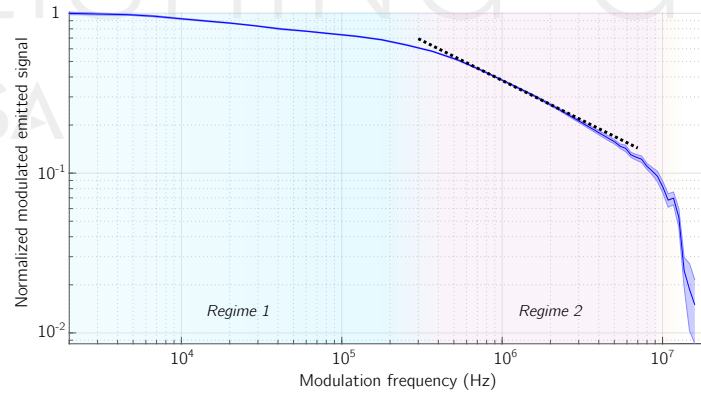


Fig. 3. Measured frequency response of the source normalized to the modulated intensity emitted at 2 kHz. The modulation frequency is $f_{\text{th}} = 2f_{\text{elec}}$. Errorbars represent $1-\sigma$ errorbars. The black dotted line indicates a $1/\sqrt{f_{\text{th}}}$ behavior fitted on the experimental data. The pink shaded area corresponds to this frequency regime whereas the blue shaded area corresponds to a constant frequency regime.

174 2.4. Polarimetric characterization

175 The polarization state of partially polarized light is best described by its Stokes vector
 176 $\mathbf{S}(\lambda) = [S_0(\lambda), S_1(\lambda), S_2(\lambda), S_3(\lambda)]$ whose components are defined as $S_0 = \langle |E_x|^2 + |E_y|^2 \rangle$,
 177 $S_1 = \langle |E_x|^2 - |E_y|^2 \rangle$, $S_2 = 2\text{Re}\langle (E_x E_y^*) \rangle$, $S_3 = -2\text{Im}\langle (E_x E_y^*) \rangle$ where the brackets denote

178 statistical average. E_x and E_y denote the projection of the electric field along the x and y
 179 axes represented in Fig. 1. The Stokes parameters contain information on the correlation
 180 between orthogonal components of the electric field and can be measured by performing intensity
 181 measurements. In particular, S_0 is proportional to the time averaged z -component of the Poynting
 182 vector $I_{\text{tot}} = \epsilon_0 c S_0 / 2$. $S_1 = I_x - I_y$ and $S_2 = I_{45^\circ} - I_{-45^\circ}$ are the difference of intensities
 183 corresponding to fields polarized along the x and y directions, along two axes rotated by 45° and
 184 -45° with respect to the x axis respectively and $S_3 = I_{\text{RCP}} - I_{\text{LCP}}$ is the difference of intensity
 185 between the RCP and LCP components. These measurements are easily done for one wavelength
 186 with a polarizer and a quarter-wave plate. In practice, the retarder behaves as a quarter waveplate
 187 only for a given wavelength. When working at other wavelengths, the retardance differs and
 188 analysis of circular polarization states is no longer straightforward. Still, the Stokes vector can
 189 be retrieved provided that the Mueller matrix of the waveplate is fully characterized and for
 190 wavelengths such that the waveplate does not behave as a $n\pi$ retarder. The general procedure
 191 developed to extract the Stokes vector from a set of 5 independent measurements is briefly
 192 described in the supplemental document.

193 With this method, the Stokes vector can be recovered over a spectral range spanning from 3.5
 194 μm to 8 μm . Fig. 4 shows the measured Stokes vector of the emitted light normalized by the
 total intensity as a function of wavelength. The corresponding DOP is plotted in Fig. 5.

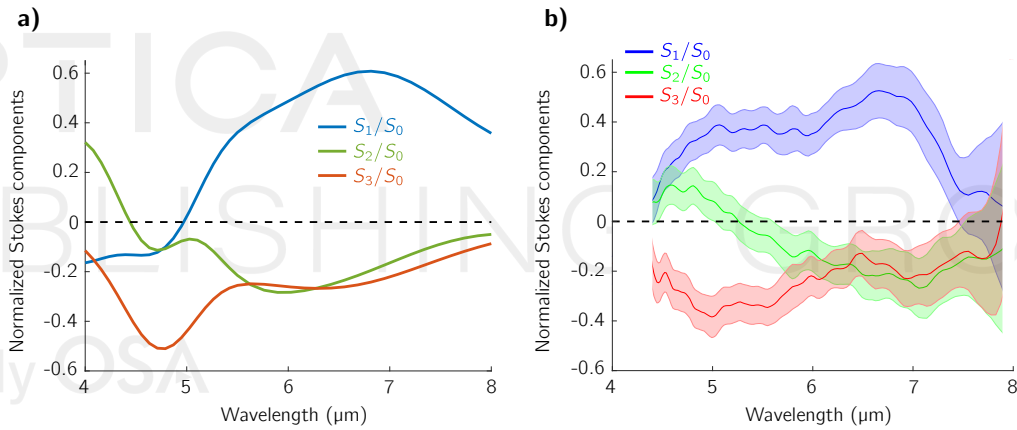


Fig. 4. Calculated (left) and experimentally measured (right) normalized Stokes parameters of the metasurface emission. The S_3 component is reversed in the simulation to allow comparison with the experimental results. Discontinuity around $4.2 \mu\text{m}$ in the experimental plot accounts for the CO_2 absorption line. Shaded areas represent $1-\sigma$ errorbars.

195
 196 The experimental observations can be compared to simulations. Absorption of a plane wave
 197 under normal incidence with linear and circular polarizations is computed to obtain $S_0 = A_x + A_y$,
 198 $S_1 = A_x - A_y$, $S_2 = A_{45^\circ} - A_{-45^\circ}$ and $S_3 = -(A_{\text{RCP}} - A_{\text{LCP}})$ where A_v is the absorption of a
 199 v -polarized plane wave under normal incidence. Note the minus sign affecting the S_3 component
 200 due to the inversion of helicity of light which depends on the direction of propagation and is
 201 therefore reversed between emission and absorption.

202 Experimental results are in fair agreement with the simulations. As seen in Fig. 4a, the
 203 surface was designed to present a peak in S_3 at $4.7 \mu\text{m}$. We indeed observe a peak in S_3
 204 of -0.4 at $5 \mu\text{m}$. From the knowledge of the Stokes vector, we can extract the degree of
 205 polarization $\text{DOP} = \sqrt{S_1^2 + S_2^2 + S_3^2} / S_0$ of the source as well as its degree of circular polarization
 206 $\text{DOCP} = |S_3 / S_0|$, as shown in Fig. 5. We have therefore characterized the incandescent source
 207 as emitting above 40% of polarized radiation with an elliptic polarization on a spectral range

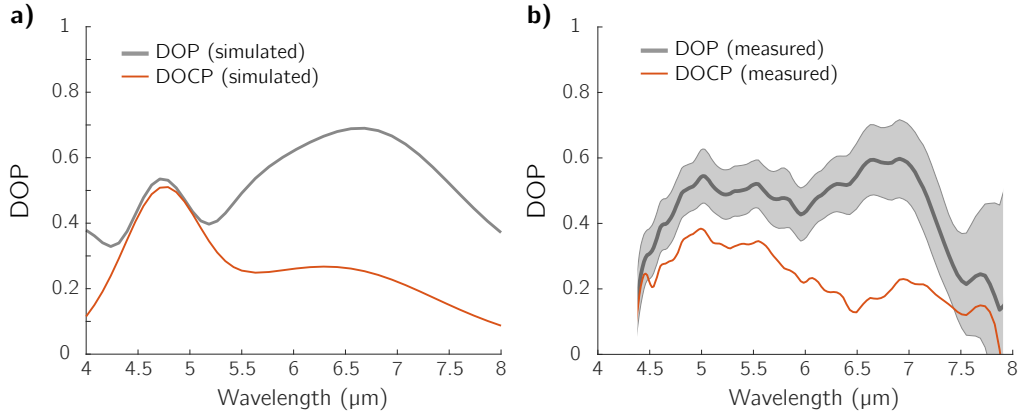


Fig. 5. a) Simulated and b) measured degree of polarization (DOP) and degree of circular polarization (DOCP). Shaded areas represent one-sigma errorbars.

208 extending from 4.6 μm to 7.2 μm , with a maximum reaching 60%. Although the polarized part
 209 of the emission is predicted to be close to purely circular at 4.7 μm , experimental characterization
 210 shows an additional linear dichroism in the 4.5-5.5 μm range. All these results are analysed in
 211 the next section.

212 3. Discussion

213 3.1. Absorption mapping depending on polarization

214 To investigate the origin of the large degree of circular polarization around 5 μm , we start by
 215 comparing the mapping of the local absorption in the platinum structure when it is illuminated
 216 by a left or right circular polarization. Fig. 6a shows a map of the local absorption inside
 217 the platinum for each polarization at $\lambda_0 = 4.7 \mu\text{m}$. Absorption is much larger for left circular
 218 polarization and occurs mainly in the constrictions. From the local Kirchhoff's law, it follows
 219 that LCP radiation is emitted mostly by the constrictions confirming that the z-shaped structure
 220 plays an important role.

221 3.2. Modal description

222 To have a better understanding of the origin of the absorption contrast depending on the
 223 polarization of the incident plane wave, we investigate the modes of the chiral metasurface. An
 224 appropriate theoretical tool for such open and lossy systems is the quasi-normal mode (QNM)
 225 formalism. Most generally, the electromagnetic fields can be written as

$$\Psi^{(\ell)}(\mathbf{r}, \omega) = \Psi_b^{(\ell)}(\mathbf{r}, \omega) + \Psi_s^{(\ell)}(\mathbf{r}, \omega) \quad (2)$$

226 where (ℓ) stands for the polarization, $\Psi = [\mathbf{E}, \mathbf{H}]$ is the total field, $\Psi_b = [\mathbf{E}_b, \mathbf{H}_b]$ is the
 227 background field satisfying source-free Maxwell equations in the absence of the perturbation, i.e.
 228 the permittivity at the location of the resonators is replaced by the permittivity in the medium
 229 surrounding the perturbation $\varepsilon_b(\omega)$. $\Psi_s = [\mathbf{E}_s, \mathbf{H}_s]$ is the field scattered by the perturbation that
 230 has a permittivity $\Delta\varepsilon(\omega)$. The scattered electromagnetic fields can be expanded as [37]

$$\Psi_s^{(\ell)}(\mathbf{r}, \omega) \simeq \sum_{m=1}^M \alpha_m^{(\ell)}(\omega) \hat{\Psi}_m(\mathbf{r}) \quad (3)$$

231 where $\hat{\Psi}_m = [\hat{\mathbf{E}}_m, \hat{\mathbf{H}}_m]$ is a normalized QNM corresponding to pole $\tilde{\omega}_m$ of the scattering matrix,
 232 $\alpha_m^{(\ell)}(\omega)$ is the polarized complex excitation coefficient weighting the contribution of the QNM

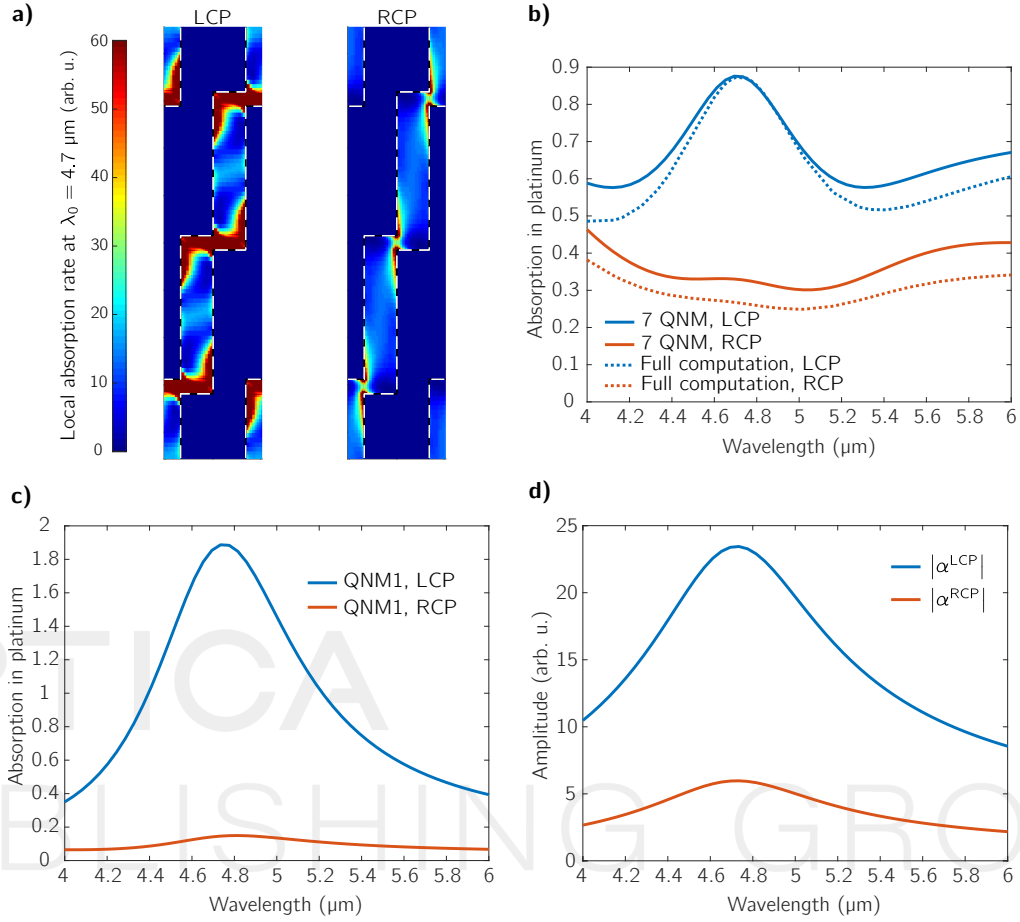


Fig. 6. a) Local absorption rate $\pi/\lambda_0\sqrt{\epsilon_0/\mu_0} \text{Im} [\epsilon(\mathbf{r}, \lambda_0)] |\mathbf{E}^{(\ell)}(\mathbf{r}, \lambda_0)|^2$ of a LCP/RCP plane wave under normal incidence at $\lambda_0 = 4.7 \mu\text{m}$. The colormap is identical for both polarizations. b) Simulated absorption in platinum illuminated by an LCP/RCP polarized plane wave as the field is truncated to 7 QNMs. c) Simulated absorption in platinum illuminated by an LCP/RCP polarized plane wave as the field is truncated to QNM1 only. Due to the truncation, i.e. the absence of interference between QNMs, absorption may be larger than 1. d) Norm of the LCP/RCP excitation coefficients for QNM1.

233 labeled m and solely depends of the frequency and M is the minimum number of QNMs needed
 234 to reach convergence.

235 To grasp the physics taking place around $5 \mu\text{m}$ leading to the circular dichroism, we look for
 236 the dominant QNM in this spectral range and consider their weight in the scattered fields. The
 237 excitation coefficient can be written as [38]:

$$\alpha_m^{(\ell)}(\omega) = \frac{\omega}{\tilde{\omega}_m - \omega} \int_V \Delta\epsilon(\mathbf{r}, \omega) \mathbf{E}_b^{(\ell)}(\mathbf{r}, \omega) \cdot \hat{\mathbf{E}}_m(\mathbf{r}) d^3\mathbf{r} \quad (4)$$

238 where V is the geometric volume of the perturbation. Equation (4) is valid provided that the
 239 so-called normalization condition is fulfilled. Normalization of the QNM is done here according
 240 to the procedure proposed by [37]. Numerical simulations of our system were performed in
 241 two main steps. First, the metasurface is reduced to a homogeneous platinum layer with same

242 thickness of 25 nm, i.e. the unperturbed configuration is a simple Salisbury screen, and the
243 corresponding background field is computed. Then, the resonant structures are added as a
244 perturbation. In our case air holes drilled through the homogeneous platinum so as to recover the
245 metasurface in Fig. 1b). When excited by the background field, these perturbations give rise to a
246 scattered field Ψ_S . Volume V for the integration in Equation (4) is thus the volume of the air
247 holes in the metasurface. Further details on the normalization of the QNM and the derivation of
248 the excitation coefficients can be found in the supplemental document.

249 A precise reconstruction of the absorption spectrum would require considering several QNMs
250 and static modes as well [39] to guarantee energy conservation. However, a good approximation
251 is obtained for 7 QNMs, as shown in Fig. 6b. Among the identified QNMs, the mode labelled
252 QNM1, (see Fig. S1 in the supplemental), is dominant and responsible for the CD around 4.7
253 μm . Fig. 6c represents the absorption spectrum in the metallic resonators when using this single
254 QNM. It is seen that the spectral dependence of the contribution of QNM1 accounts for most of
255 the circular polarization absorption. Hence, we attribute the generation of CD to the thermal
256 excitation of this particular QNM. In spite of absorption exceeding unity, it is informative to see
257 that this single QNM induces a large CD by itself. Fig. 6d shows the norm of the LCP and RCP
258 excitation coefficient of QNM1. Around 4.7 μm , the RCP coupling amplitude is nearly 5 times
259 larger than the LCP coupling, which is at the origin of the CD. QNM1 is therefore better coupled
260 to one circular polarization in the normal direction compared to the cross polarization.

261 A second QNM, labelled QNM2, has been identified. The corresponding pole lies close to
262 QNM1. In contrast with QNM1, QNM2 shows a strong linear dichroism (see Supplemental for
263 further discussion). Deviation to theory in the [4.5 - 5.5] μm range, as seen in Fig. 4, is attributed
264 to a spectral shift of the poles caused by fabrication defects of the platinum structure.

265 4. Conclusion

266 In summary, we have built a submicrometer thick source based on a chiral metasurface. Upon
267 heating, it emits elliptically polarized light over a broad spectral range. The emission has a
268 high DOP reaching up to 0.54 at 5 μm , with a degree of circular polarization as high as 0.38.
269 The design of the source relies on chiral sub-units that have modes coupling efficiently to one
270 circular polarization and poorly to the other. Optimization of the source requires a control over
271 its polarized emissivity as well as over the distribution of temperature elevation throughout the
272 structure. Thanks to the source architecture, modulation up to 10 MHz of the emission can be
273 achieved through temperature modulation of the source, relying on heat conduction to a colder
274 underlying substrate. The device presented in this work enables to control the polarization and
275 spectrum of the emitted radiation indicating that incandescent metasurfaces offer a versatile
276 platform for MWIR emission.

277 **Author contributions** J.-J.G. proposed and supervised the project. A.N. designed and
278 fabricated the device. A.-L.C. participated in the device fabrication. A.N. performed the
279 numerical simulations. J.-P. H. participated in the numerical simulations. A.N. and E.G.-C.
280 designed the experimental setup. E.G.-C. and B.V. advised on the choice of polarization optical
281 elements. A.N. performed the device characterization and analyzed the data. A.N. and J.-J.G.
282 wrote the paper with input from all authors.

283 **Funding** This work was supported by the grant ANR-17-CE24-016 of the Agence Nationale
284 de la Recherche.

285 **Acknowledgments** A. N. acknowledges support from Direction Générale de l'Armement.

286 **Disclosures** The authors declare no conflicts of interest.

287 **Data availability** Data can be found in the repository 10.5281/zenodo.7478341.

288 **References**

- 289 1. T.-H. Chiou, S. Kleinlogel, T. Cronin, R. Caldwell, B. Loeffler, A. Siddiqi, A. Goldizen, and J. Marshall, "Circular
290 Polarization Vision in a Stomatopod Crustacean," *Curr. Biol.* **18**, 429–434 (2008).
- 291 2. Y. Gagnon, R. Templin, M. How, and N. Marshall, "Circularly Polarized Light as a Communication Signal in Mantis
292 Shrimps," *Curr. Biol.* **25**, 3074–3078 (2015).
- 293 3. L. A. Nafie, "Vibrational Circular Dichroism: A New Tool for the Solution-State Determination of the Structure and
294 Absolute Configuration of Chiral Natural Product Molecules," *Nat. Prod. Commun.* **3**, 1934578X0800300 (2008).
- 295 4. L. Wojszvyk, A. Nguyen, A.-L. Coutrot, C. Zhang, B. Vest, and J.-J. Greffet, "An incandescent metasurface for
296 quasimonochromatic polarized mid-wave infrared emission modulated beyond 10 MHz," *Nat. Commun.* **12**, 1492
297 (2021). Number: 1 Publisher: Nature Publishing Group.
- 298 5. Y. Luo, C. Chi, M. Jiang, R. Li, S. Zu, Y. Li, and Z. Fang, "Plasmonic Chiral Nanos-
299 tructures: Chiroptical Effects and Applications," *Adv. Opt. Mater.* **5**, 1700040 (2017). [_eprint:
300 https://onlinelibrary.wiley.com/doi/pdf/10.1002/adom.201700040](https://onlinelibrary.wiley.com/doi/pdf/10.1002/adom.201700040).
- 301 6. J. T. Collins, C. Kuppe, D. C. Hooper, C. Sibilina, M. Centini, and V. K. Valev, "Chirality and Chiroptical Effects
302 in Metal Nanostructures: Fundamentals and Current Trends," *Adv. Opt. Mater.* **5**, 1700182 (2017). [_eprint:
303 https://onlinelibrary.wiley.com/doi/pdf/10.1002/adom.201700182](https://onlinelibrary.wiley.com/doi/pdf/10.1002/adom.201700182).
- 304 7. W. Li and S. Fan, "Nanophotonic control of thermal radiation for energy applications," *Opt. Express* **26**, 15995–16021
305 (2018).
- 306 8. A. Chutinan and S. Noda, "Spiral three-dimensional photonic-band-gap structure," *Phys. Rev. B* **57**, R2006–R2008
307 (1998).
- 308 9. M. Thiel, M. Decker, M. Deubel, M. Wegener, S. Linden, and G. von Freymann, "Polarization Stop
309 Bands in Chiral Polymeric Three-Dimensional Photonic Crystals," *Adv. Mater.* **19**, 207–210 (2007). [_eprint:
310 https://onlinelibrary.wiley.com/doi/pdf/10.1002/adma.200601497](https://onlinelibrary.wiley.com/doi/pdf/10.1002/adma.200601497).
- 311 10. J. K. Gansel, M. Thiel, M. S. Rill, M. Decker, K. Bade, V. Saile, G. v. Freymann, S. Linden, and M. Wegener,
312 "Gold Helix Photonic Metamaterial as Broadband Circular Polarizer," *Science* **325**, 1513–1515 (2009). Publisher:
313 American Association for the Advancement of Science Section: Report.
- 314 11. M. Rajaei, J. Zeng, M. Albooyeh, M. Kamandi, M. Hanifeh, F. Capolino, and H. K. Wickramasinghe, "Giant Circular
315 Dichroism at Visible Frequencies Enabled by Plasmonic Ramp-Shaped Nanostructures," *ACS Photonics* **6**, 924–931
316 (2019). Publisher: American Chemical Society.
- 317 12. J. C. W. Lee and C. T. Chan, "Circularly polarized thermal radiation from layer-by-layer photonic crystal structures,"
318 *Appl. Phys. Lett.* **90**, 051912 (2007).
- 319 13. M. Thiel, G. v. Freymann, and M. Wegener, "Layer-by-layer three-dimensional chiral photonic crystals," *Opt. Lett.,*
320 *OL* **32**, 2547–2549 (2007). Publisher: Optical Society of America.
- 321 14. M. Decker, R. Zhao, C. M. Soukoulis, S. Linden, and M. Wegener, "Twisted split-ring-resonator photonic metamaterial
322 with huge optical activity," *Opt. Lett.* **35**, 1593–1595 (2010).
- 323 15. Y. Zhao, M. A. Belkin, and A. Alù, "Twisted optical metamaterials for planarized ultrathin broadband circular
324 polarizers," *Nat. Commun.* **3**, 870 (2012). Number: 1 Publisher: Nature Publishing Group.
- 325 16. A. Papakostas, A. Potts, D. M. Bagnall, S. L. Prosvirnin, H. J. Coles, and N. I. Zheludev, "Optical Manifestations of
326 Planar Chirality," *Phys. Rev. Lett.* **90**, 107404 (2003).
- 327 17. S. L. Wadsworth and G. D. Boreman, "Broadband infrared meanderline reflective quarter-wave plate," *Opt. Express,*
328 *OE* **19**, 10604–10612 (2011). Publisher: Optical Society of America.
- 329 18. C. Wu, N. Arju, G. Kelp, J. A. Fan, J. Dominguez, E. Gonzales, E. Tutuc, I. Brener, and G. Shvets, "Spectrally
330 selective chiral silicon metasurfaces based on infrared Fano resonances," *Nat. Commun.* **5**, 3892 (2014). Number: 1
331 Publisher: Nature Publishing Group.
- 332 19. E. Briones, A. Cuadrado, J. Briones, R. D. d. León, J. C. Martínez-Antón, S. McMurtry, M. Hehn, F. Montaigne,
333 J. Alda, and F. J. González, "Seebeck nanoantennas for the detection and characterization of infrared radiation," *Opt.*
334 *Express, OE* **22**, A1538–A1546 (2014). Publisher: Optical Society of America.
- 335 20. W. Li, Z. J. Coppens, L. V. Besteiro, W. Wang, A. O. Govorov, and J. Valentine, "Circularly polarized light detection
336 with hot electrons in chiral plasmonic metamaterials," *Nat. Commun.* **6**, 8379 (2015). Number: 1 Publisher: Nature
337 Publishing Group.
- 338 21. W. Liu, L. Mei, Y. Li, L. Yu, Z. Lai, T. Yu, and H. Chen, "Controlling the spin-selective absorption with two-
339 dimensional chiral plasmonic gratings," *Opt. Lett., OL* **44**, 5868–5871 (2019). Publisher: Optical Society of
340 America.
- 341 22. L. Ouyang, W. Wang, D. Rosenmann, D. A. Czaplewski, J. Gao, and X. Yang, "Near-infrared chiral plasmonic
342 metasurface absorbers," *Opt. Express, OE* **26**, 31484–31489 (2018). Publisher: Optical Society of America.
- 343 23. S. L. Wadsworth, P. G. Clem, E. D. Branson, and G. D. Boreman, "Broadband circularly-polarized infrared emission
344 from multilayer metamaterials," *Opt. Mater. Express* **1**, 466 (2011).

- 345 24. J.-J. Greffet, R. Carminati, K. Joulain, J.-P. Mulet, S. Mainguy, and Y. Chen, "Coherent emission of light by thermal
346 sources," *Nature* **416**, 61–64 (2002).
- 347 25. S. Takahashi, Y. Ota, T. Tajiri, J. Tatebayashi, S. Iwamoto, and Y. Arakawa, "Circularly polarized vacuum field in
348 three-dimensional chiral photonic crystals probed by quantum dot emission," *Phys. Rev. B* **96**, 195404 (2017). ArXiv:
349 1707.04996.
- 350 26. A. A. Maksimov, I. I. Tartakovskii, E. V. Filatov, S. V. Lobanov, N. A. Gippius, S. G. Tikhodeev, C. Schneider,
351 M. Kamp, S. Maier, S. Höfling, and V. D. Kulakovskii, "Circularly polarized light emission from chiral spatially-
352 structured planar semiconductor microcavities," *Phys. Rev. B* **89**, 045316 (2014). Publisher: American Physical
353 Society.
- 354 27. K. Konishi, M. Nomura, N. Kumagai, S. Iwamoto, Y. Arakawa, and M. Kuwata-Gonokami, "Circularly Polarized
355 Light Emission from Semiconductor Planar Chiral Nanostructures," *Phys. Rev. Lett.* **106**, 057402 (2011).
- 356 28. A. C. Overvig, S. A. Mann, and A. Alù, "Thermal Metasurfaces: Complete Emission Control by Combining Local
357 and Nonlocal Light-Matter Interactions," *Phys. Rev. X* **11**, 021050 (2021). Publisher: American Physical Society.
- 358 29. N. Dahan, Y. Gorodetski, K. Frischwasser, V. Kleiner, and E. Hasman, "Geometric Doppler Effect: Spin-Split
359 Dispersion of Thermal Radiation," *Phys. Rev. Lett.* **105**, 136402 (2010).
- 360 30. J. Ginn, D. Shelton, P. Krenz, B. Lail, and G. Boreman, "Polarized infrared emission using frequency selective
361 surfaces," *Opt. Express*, *OE* **18**, 4557–4563 (2010). Publisher: Optical Society of America.
- 362 31. X. Wang, T. Sentz, S. Bharadwaj, S. Ray, Y. Wang, D. Jiao, L. Qi, and Z. Jacob, "Observation of non-vanishing
363 optical helicity in thermal radiation from symmetry-broken metasurfaces," (2022).
- 364 32. G. Kirchhoff, "On the relation between the radiating and absorbing powers of different bodies for light and heat," *The
365 London, Edinburgh, Dublin Philos. Mag. J. Sci.* **20**, 1–21 (1860).
- 366 33. S. Bauer, "Optical properties of a metal film and its application as an infrared absorber and as a beam splitter," *Am. J.
367 Phys.* **60**, 257–261 (1992).
- 368 34. J.-J. Greffet, P. Bouchon, G. Brucoli, and F. Marquier, "Light Emission by Nonequilibrium Bodies: Local Kirchhoff
369 Law," *Phys. Rev. X* **8**, 021008 (2018). Publisher: American Physical Society.
- 370 35. P. Barritault, M. Brun, S. Gidon, and S. Nicoletti, "Mid-IR source based on a free-standing microhotplate for
371 autonomous CO₂ sensing in indoor applications," *Sensors Actuators A: Phys.* **172**, 379–385 (2011).
- 372 36. A. Nguyen and J.-J. Greffet, "Efficiency optimization of mid-infrared incandescent sources with time-varying
373 temperature," *Opt. Mater. Express* **12**, 225 (2022).
- 374 37. Q. Bai, M. Perrin, C. Sauvan, J.-P. Hugonin, and P. Lalanne, "Efficient and intuitive method for the analysis of light
375 scattering by a resonant nanostructure," *Opt. Express* **21**, 27371 (2013).
- 376 38. P. Lalanne, W. Yan, K. Vynck, C. Sauvan, and J.-P. Hugonin, "Light Interaction with
377 Photonic and Plasmonic Resonances," *Laser & Photonics Rev.* **12**, 1700113 (2018). [_eprint:
378 https://onlinelibrary.wiley.com/doi/pdf/10.1002/lpor.201700113](https://onlinelibrary.wiley.com/doi/pdf/10.1002/lpor.201700113).
- 379 39. C. Sauvan, "Quasinormal modes expansions for nanoresonators made of absorbing dielectric materials: study of the
380 role of static modes," *Opt. Express* **29**, 8268 (2021).